HHS Public Access

Author manuscript

Cell Rep. Author manuscript; available in PMC 2020 September 03.

Published in final edited form as:

Cell Rep. 2018 June 26; 23(13): 3878–3890. doi:10.1016/j.celrep.2018.05.091.

Synchronized Astrocytic Ca^{2+} Responses in Neurovascular Coupling during Somatosensory Stimulation and for the Resting State

Xiaochun Gu[1,2], **Wei Chen**[1], **Nora D. Volkow**[3], **Alan P. Koretsky**[4], **Congwu Du**[1], **Yingtian Pan**[1,5,*]

[1]Department of Biomedical Engineering, Stony Brook University, Stony Brook, NY 11794, USA

[2]Jiangsu Key Laboratory of Molecular and Functional Imaging, Key Laboratory of Developmental Genes and Human Diseases, Department of Radiology, Zhongda Hospital, Medical School, Southeast University, #87 Dingjiaqiao Road, Nanjing 210009, China

[3]National Institute on Alcohol Abuse and Alcoholism, NIH, Bethesda, MD 20857, USA

[4]Laboratory of Functional and Molecular Imaging, National Institute of Neurological Disorders and Stroke, NIH, Bethesda, MD 20892, USA

[5]Lead Contact

SUMMARY

The role of astrocytes in neurovascular coupling (NVC) is unclear. Here, we applied a multimodality imaging approach to concomitantly measure synchronized neuronal or astrocytic Ca^{2+} and hemodynamic changes in the mouse somatosensory cortex at rest and during sensory electrical stimulation. Strikingly, we found that low-frequency stimulation (0.3–1 Hz), which consistently evokes fast neuronal Ca^{2+} transients (6.0 ± 2.7 ms latency) that always precede vascular responses, does not always elicit astrocytic Ca^{2+} transients (313 ± 65 ms latency). However, the magnitude of the hemodynamic response is increased when astrocytic transients occur, suggesting a facilitatory role of astrocytes in NVC. High-frequency stimulation (5–10 Hz) consistently evokes a large, delayed astrocytic Ca^{2+} accumulation (3.48 ± 0.09 s latency) that is temporarily associated with vasoconstriction, suggesting a role for astrocytes in resetting NVC. At rest, neuronal, but not astrocytic, Ca^{2+} fluctuations correlate with hemodynamic low-frequency oscillations. Taken together, these results support a role for astrocytes in modulating, but not triggering, NVC.

*Correspondence: yingtian.pan@stonybrook.edu.

AUTHOR CONTRIBUTIONS

X.G., C.D., and Y.P. designed the research. X.G. and W.C. carried out the experiments and data analysis. X.G., C.D., Y.P., N.D.V., and A.P.K. contributed significantly to data interpretation, discussion of the results, and writing of the manuscript.

SUPPLEMENTAL INFORMATION

Supplemental Information includes Supplemental Experimental Procedures, seven figures, and one table and can be found with this article online at https://doi.org/10.1016/j.celrep.2018.05.091.

DECLARATION OF INTERESTS

The authors declare no competing interests.

Graphical Abstract

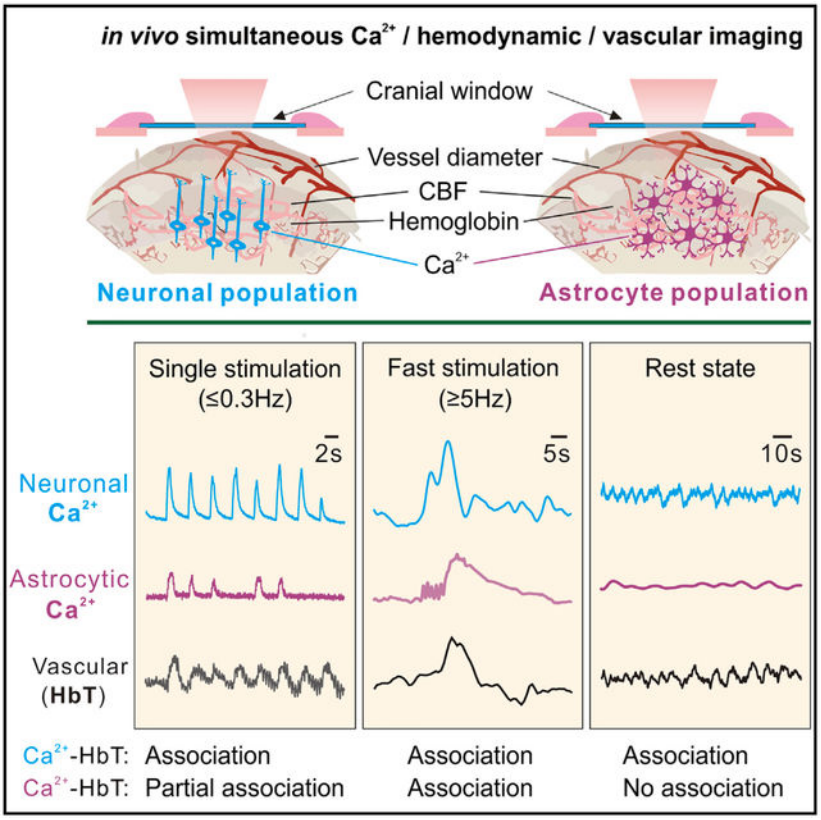

In Brief

Using concomitant multimodality optical imaging of synchronized neuronal or astrocytic Ca^{2+} and hemodynamic changes, Gu et al. show hemodynamic responses to slow sensory stimuli without astrocytic Ca^{2+} changes. Astrocytic Ca^{2+} correlates with vasoconstriction after fast stimuli. Neuronal, not astrocytic, slow Ca^{2+} fluctuations correlate with hemodynamics at rest.

INTRODUCTION

Neurovascular coupling (NVC) is a process by which brain regions control blood flow to meet the demands of changes in neuronal activity. There is still no broad consensus on the mechanism underlying NVC. Of particular interest has been the role neurons and astrocytes that may play in triggering NVC. Some studies have shown that neurons can be the driving force behind NVC during stimulation-induced changes in hemodynamics (Attwell and Laughlin, 2001; O'Herron et al., 2016), and others have focused on the role of astrocytes (Mishra et al., 2016). Studies assessing the role of astrocytes in NVC have measured intracellular Ca^{2+} as a marker of activity and have shown that Ca^{2+} elevation in astrocytes is associated with release of vasoactive compounds that might drive blood flow changes in NVC (Girouard et al., 2010; Metea and Newman, 2006; Mulligan and MacVicar, 2004; Takano et al., 2006a). However, the role of astrocytes in NVC was recently questioned because the Ca^{2+} transients evoked in astrocytes in response to neuronal activity were sparse

and delayed relative to the onset of functional hyperemia (Schulz et al., 2012; Schummers et al., 2008; Wang et al., 2006). In addition, NVC persisted in IP3R2 knockout mice (Nizar et al., 2013), in whom Ca^{2+} signaling in astrocytes is inhibited, which has been interpreted to suggest that astrocytes are not involved in NVC during stimulation-induced changes in hemodynamics.

The lack of consensus is likely due to the large range of stimulations used, the complexity of astrocytic Ca^{2+} changes, and the fact that most studies used high-resolution microscopy, which restricts imaging to very small fields of view (FOVs). Moreover, most studies that monitored Ca^{2+} signals only captured Ca^{2+} transients occurring in the soma triggered by strong stimulation (Haustein et al., 2014). These studies may have missed Ca^{2+} signals in astrocyte processes associated with nearby overlapping synapses (Di Castro et al., 2011; Panatier et al., 2011). Indeed, *in vivo* evidence using genetically encoded calcium inidicators (GECIs) (e.g., GCaMP6f) has shown that Ca^{2+} signals in astrocytes are highly compartmentalized and that the activity in discrete regions or microdomains can be uncorrelated with that occurring in the soma (Otsu et al., 2015; Srinivasan et al., 2015). This indicates that astrocytic Ca^{2+} dynamics may be more complex than typically assumed. Noteworthy is the fact that these Ca^{2+} signaling studies were conducted at single-astrocyte cell level within a small FOV accessible by two-photon confocal microscopy rather than over the cell population from which synchronized Ca^{2+} signaling arises (Kuga et al., 2011; Nimmerjahn et al., 2009; Paukert et al., 2014). Indeed, the behavior of synchronized Ca^{2+} signaling from large-scale astrocyte populations is not well understood and neither is their functional role in NVC.

Large-scale synchronized activity from cell populations is likely to play an important role in NVC. Increases in cerebral blood flow (CBF) triggered by sensory stimulation (functional hyperemia) reflect flow changes occurring simultaneously among several blood vessels over the stimulated brain region (Pan et al., 2014). Previous *in vivo* studies in the rodent cortex showed that astrocytes in the stimulated region tend to exhibit synchronized Ca^{2+} elevations (Hirase et al., 2004; Takata and Hirase, 2008). Astrocytes are highly interconnected and organized as a syncytium in which individuals occupying distinct domains are extensively coupled through gap junctions (Giaume et al., 2010; Nimmerjahn and Bergles, 2015), and it is unclear how astrocyte networks are controlled when engaging in NVC (Nuriya and Hirase, 2016; Rosenegger and Gordon, 2015). Similarly, large-scale synchronized cellular activation (assessed with Ca^{2+} indicators) is highly correlated with the spontaneous slow functional hemodynamic oscillations detected with fMRI (assessed with blood oxygen level-dependent [BOLD] or perfusion techniques) during the resting state (Du et al., 2014). Although there is consistent evidence of neuronal involvement in stimulation-induced BOLD changes (Logothetis, 2008) and of the slow BOLD oscillations used to measure resting functional connectivity with fMRI (Schölvinck et al., 2010; Shmuel and Leopold, 2008), the involvement of astrocytes is less clear. No study has evaluated the interactions between synchronized astrocytic Ca^{2+} signals and NVC during stimulation-induced changes in hemodynamics or during resting spontaneous hemodynamic fluctuations.

To address the role of astrocytes in NVC both during stimulation and at rest, synchronized Ca^{2+} activity for a large area of the hindpaw somatosensory cortex was measured from

astrocytes and neurons along with the associated hemodynamic changes in the mouse brain. A viral injection of GCaMP6f (Chen et al., 2013; Haustein et al., 2014) into the somatosensory cortex of cre transgenic mice enabled either neuron-specific or astrocyte-specific Ca^{2+} expression. A multimodality imaging platform (MIP) through a chronic cranial window (Gu et al., 2018) was applied to enable acquisition of cell-specific Ca^{2+} changes from astrocytes or neurons while concurrently measuring dynamic changes in cerebral blood flow velocity (CBFv), blood volume (total hemoglobin concentration [HbT]), and vascular dilation separately for veins and arteries at high spatiotemporal resolutions and over a relatively large FOV. We show that the synchronized astrocytic Ca^{2+} responses to low-frequency sensory stimulations were weaker, slower, less consistent, and longer-lasting than the synchronized neuronal Ca^{2+} responses, whereas, for high-frequency stimulation, the astrocytic Ca^{2+} responses were cumulative and consistent but longer-lasting than the cumulative neuronal Ca^{2+} responses and persisted after the end of stimulation. More importantly, our findings suggest a facilitatory and resetting role of astrocytes in NVC during stimulation. However, at rest under physiological conditions, astrocytic Ca^{2+} fluctuations do not seem to contribute to hemodynamic low-frequency oscillations, which, instead, are driven by neuronal oscillations, although they might participate when hemodynamics are disrupted; for example, during hypercapnia.

RESULTS

Genetic Expression of GCaMP6f in Neurons and Astrocytes

To define the mechanisms by which astrocytic and neuronal activities are involved in NVC *in vivo*, we used a viral injection strategy to express a genetically encoded Ca^{2+} indicator, GCaMP6f, in mice in a cell-specific manner (Figures 1B and 1E). For neuronal expression, we injected AAV5-syn-GCaMP6f (AV-5-PV2822, Penn Vector Core) into the hindpaw region of the somatosensory cortex in wild-type C57 mice (Figure 1B). After 4 weeks, GCaMP6f was expressed in 47.9% ± 2.6% of cortical neurons (n = 6 mice) (Figures 1C–1D'). *Ex vivo* confirmation via double staining with NeuN antibody to label neurons and GFP antibody to label GCaMP6f showed that all GFP_+ cells were neurons. No GCaMP6f cells that were glial fibrillary acidic protein ($GFAP_+$) were detected (Figure S1). For astrocyte expression, we injected AAV5-Flex-GCaMP6f (AV-5-PV2816, Penn Vector Core) into the same brain region in GFAP-Cre mice (Jax 024098). Cre recombination induced GCaMP6f expression in 45.2% ± 4.5% of cortical astrocytes (n = 6 mice) after 4 weeks of injection (Figures 1F–1G'), which could be visualized *in vivo* using our MIP through a cranial window (Figures 1A and 1H). Double staining with GFAP antibody to label astrocytes and GFP antibody to label GCaMP6f showed that the GFP+ cells were all astrocytes; consistently, these GCaMP6f cells were not $NeuN_+$ (Figure S1). It must be noted that, unlike previously reported dye labeling routes (Takano et al., 2006a), GCaMP6f was expressed in both the soma and the processes of astrocytes (yellow arrows and white arrowheads in Figures 1G' and S1), facilitating simultaneous characterization of different regional synchronized Ca^{2+} dynamics from the astrocyte population (e.g., processes versus somata) (Shigetomi et al., 2013, 2016).

Frequency Dependence of Synchronized Neuronal and Astrocytic Ca^{2+} Dynamics

Synchronized Ca^{2+} transients from cortical neuronal and astrocyte populations were measured under different stimulation frequencies (e.g., 0.3 Hz, 1 Hz, 3 Hz, 5 Hz, and 10 Hz). For neurons, when the stimulation frequency was slow (0.3 Hz and 1 Hz), the synchronized Ca^{2+} transient corresponded one to one with each single stimulation. When the frequency was increased to 3 Hz, sometimes a stimulation did not lead to a Ca^{2+} response (Figures 2A and 2B). For the higher frequencies (5 Hz and 10 Hz), the GCaMP6f signal could not keep up with the neuronal ensemble response, and there was cumulative Ca^{2+} elevation (Figures 2C–2E). The peak Ca^{2+} amplitudes increased from 0.15% ± 0.02% for 0.3 Hz to 0.52% ± 0.05% for 1 Hz, 4.4% ± 0.1% for 3 Hz, 6.2% ± 0.2% for 5 Hz, and 7.7% ± 0.1% for 10 Hz (Figure 2K; m = 17, n = 6).

For astrocytes, the synchronized Ca^{2+} responses also showed a transition from primarily transient responses to individual stimulation at 0.3–3 Hz to mostly slow cumulative elevations at 5–10 Hz (Figures 2F–2J and 2L). Interestingly, often there was no astrocytic Ca^{2+} transient to an electrical stimulation, even at the lowest frequencies of 0.3-Hz and 1-Hz stimulation. The response rate to an electrical stimulation for neuronal Ca^{2+} was 99% ± 0.2%, and for astrocytic Ca^{2+} it was 57.73% ± 8.2% at0.3 Hz and 47.7% ± 7.0% for 1 Hz ($p < 0.001$, m = 20, n = 6, Student's t test) (Figure 2G; Figure S2). The neuronal and astrocyte responses to stimulations above 1 Hz were likely constrained by the inability of GCaMP6f to keep up with cellular dynamics for its slow off rate (Chen et al., 2013). In neurons at 3 Hz, there was some evidence of responses to individual stimulation, but there was also a slow accumulation of fluorescence. By 5 and 10 Hz, individual transients could not be detected, and a cumulative increase in fluorescence was detected. Astrocytes also exhibited a complex response when the stimulation frequency increased. At low frequency, individual stimulations could be resolved (except that, many times, a stimulation did not evoke a change in astrocyte Ca^{2+}). At high frequencies (5 and 10 Hz), some evidence of individual responses could be detected on a large increasing level of cumulative fluorescence. Two components were distinguished in the astrocyte Ca^{2+} signal: a fast component that was most visible for the lower-frequency stimulations (0.3–5 Hz) and a slow component observed at 3 Hz and higher stimulation frequencies (5–10 Hz). The fast component consisted of Ca^{2+} transients that decreased with the higher-frequency stimulations, corresponding to 3.19% ± 0.18% for 0.3 Hz (m = 18, n = 6) and 3.39% ± 0.19% for 1 Hz (m = 18, n = 6) but decreasing to 2.2% ± 0.3% for 3 Hz (m = 26, n = 6), 1.7% ±0.2% for 5 Hz (m = 17, n = 6), and 0.08% ± 0.006% for 10 Hz (m = 17, n = 6). The slow astrocytic component showed a slow Ca^{2+} accumulation that was first detected at 3 Hz and increased with the frequency of stimulation from 0.08% ± 0.02% at 3 Hz (m = 17, n = 6) to 3.3% ± 0.2% at 5 Hz (m = 17, n = 6) and to4.2% ± 0.19% at 10 Hz (m = 18, n = 6). Interestingly, astrocytic Ca^{2+} response to 5-Hz stimulation exhibited a bi-phase response; i.e., an early phase of fast transient Ca^{2+} spikes followed by a later phase of slow Ca^{2+} accumulation (Figure 2I). There was a 3.48 ± 0.09 s latency to stimulation onset of the slow cumulative astrocytic Ca^{2+} elevation, which was significantly slower than the cumulative neuronal increase in fluorescence ($p < 0.001$, m = 17, n = 6, Student's t test). This latency matches well the ~3- to 4-s delay for astrocytic somatic Ca^{2+} elevations previously reported in studies that used dye loading (Nizar et al., 2013; Schummers et al., 2008). This suggests that the slow astrocytic Ca^{2+} accumulation

component evoked by high-frequency stimulation corresponds to somatic Ca^{2+} signaling. Additionally, these results indicate that astrocytes do not always give transient Ca^{2+} responses to electrical stimulation, even for low frequencies (0.3 to 1 Hz). This is also consistent with previously published results at the single-cell level using two-photon microscopy (Haustein et al., 2014).

Single Sensory Stimulation Evoked Ca^{2+} Transients that Were Fast and Highly Synchronized for Neuronal Populations and Slower and Less Synchronized for Astrocytic Populations

To assess the neuronal and astrocytic responses to isolated stimulation, we measured the Ca^{2+} transients elicited at the lowest stimulation frequency (3 mA and 0.3 ms). The recorded neuronal Ca^{2+} transients observed for each single stimulation (Figure 3A; Figure S3) were fast and reproducible across the repeated stimulation trials (m = 20 trials, n = 5 mice). The measured latency, duration, and peak amplitude of neuronal Ca^{2+} transients were τ_N (latency of neuronal response to stimulation onset) = 6.0 ± 2.7 ms, Δt_N (duration of neuronal response) = 537 ± 34 ms, and relative florescence change $(DF/F)_N$ = 6.40% ± 0.29%, which were averaged over a region of interest (ROI) of ~diameter (ϕ) 0.5 mm (blue circle in Figure 3A).

Similarly, robust synchronized Ca^{2+} transients were detected from astrocytes in response to some of the single stimulations (e.g., 57.73% ± 8.2% of 0.3-Hz stimulations elicited an astrocytic response). Astrocyte responses were slower, longer-lasting, and smaller than neuronal responses, with a measured latency, duration, and peak amplitude of τ_A (latency of astrocyte response to stimulation onset) = 313 ± 65 ms, Δt_A (duration of astrocyte response) = 993 ± 48 ms, and $\Delta F/F_A$ = 1.74% ± 0.1% over an ROI of ~ϕ0.5 mm (Figure 3B; Figure S3) (m = 20 trials, n = 5 mice).

Comparisons between astrocytic and neuronal Ca^{2+} transients revealed significant differences. Neuronal Ca^{2+} increases occurred immediately following the stimulation onset (latency of 6.0 ± 2.7 ms), whereas astrocytic Ca^{2+} increases were delayed by 313 ± 65 ms ($p < 0.001$, Student's t test, m = 20, n = 5 mice) and were less synchronized (Figures 3A and 3B). The astrocytic Ca^{2+} transient amplitude was 72.8% ± 0.3% lower ($p < 0.001$, Student's t test, m = 20, n = 5 mice), and its duration was 84.9% ± 10.9% longer ($p < 0.001$, Mann-Whitney test, m = 20, n = 5 mice) than neuronal ones (Figures 3C–3E). It should be noted that the detected Ca^{2+} transient from the synchronized astrocyte population is different from the previously reported Ca^{2+} fluctuations at single-cell level, which were slow, sparse, and evoked only by high-frequency stimulation (Schummers et al., 2008). Our data (Figure 3B) are consistent with recent findings of a faster Ca^{2+} transient in the processes of astrocytes that expressed GCaMP6f (Otsu et al., 2015). Thus, coordinated astrocyte responses from many cells over the somatosensory cortex have been detected from a single electrical stimulation.

To assess whether astrocytes have spatially restricted responses, we measured the correlation of the transients evoked by single stimulation on 15 contiguous astrocytes and compared them with those for 15 contiguous neurons on a circular ROI (~ϕ30 mm) (Figures 3F and 3G). Analysis of the spatiotemporal correlations of Ca^{2+} changes in single cells within the

ROIs (i, j = 1,…, m) shows that the cross-correlation coefficient for neuronal Ca^{2+}, r_N = 0.966 ± 0.005 (m = 15, n = 5 mice), was significantly larger ($p < 0.001$, Mann-Whitney test) than for astrocytic Ca^{2+}, r_A = 0.638 ± 0.025 (m = 15, n = 5 mice) (Figures 3H and 3I). Furthermore, the duration (Δt_A = 953 ± 42 ms, m = 20, n = 5 mice) of synchronized astrocytic Ca^{2+} transients across the population of astrocytes (Figure 3J) evoked by stimulation was 62.6% ± 9.1% broader than that of a single astrocyte (Δt_A = 586 ± 33 ms, m = 20, n = 5 mice; Figure S4), whereas the duration (Δt_A = 484 ± 24 ms, m = 20, n = 5 mice) of synchronized neuronal Ca^{2+} transients (Figure 3J) was similar to that of a single neuron (Δt_A = 453 ± 23 ms, m = 20, n = 5 mice; Figure S4). This indicates that Ca^{2+} activation of the neuronal population is highly synchronized whereas that of the astrocyte population is much less so.

Neuronal, Not Astrocytic, Ca^{2+} Correlated with NVC to Single Sensory Stimulation

Single sensory stimulations (0.3 Hz) evoked weak, sparse astrocytic Ca^{2+} transients but highly synchronized, consistent, and strong neuronal Ca^{2+} transients (Figures 3A and 3F), which led us to compare their association with hemodynamic changes induced by single stimulation. At 0.3-Hz stimulation, neuronal Ca^{2+} reliably responded to almost all of the stimulation trials with an overall response rate of 99% ± 0.1%, whereas astrocytic Ca^{2+} responded irregularly, showing an overall response rate of 57.7% ± 8.2% across all 8 trials ($p < 0.001$, m = 20, n = 6, Student's t test) (Figures 4A and 4B). Although astrocytes consistently responded to the first 3 stimulations, their Ca^{2+} response rate declined from 84.4% ± 8.6% to 32.4% ± 10.5% for the late 7–8 stimulations in each trial ($p < 0.001$, m = 20, n = 6, repeated one-way ANOVA), and their transient amplitudes decreased from 3.03% ± 0.18% to 0.45% ± 0.19% ($p < 0.0001$, m = 12, n = 3, Student's t test) (Figures 4B, 4E, and 4F). On the other hand, the hemodynamics (e.g., ΔHbT) responded to almost all stimulations (98% ± 0.2% for the first 3 and 97% ±0.1% for the last 3 stimulations; Figure 4C), similar to the rate of the neuronal responses. Thus, the pattern of hemodynamic responses to single stimulation corresponded to that observed for neuronal but not for astrocytic transients, which indicates that neurons, and not astrocytes, are driving the individual hemodynamic responses. Interestingly, the neuronal Ca^{2+} amplitude was very consistent at the beginning or end of the stimulation train, indicating that they are independent of whether there was or there was no astrocytic Ca^{2+} response (7.2% ± 0.19% versus 6.7% ± 0.34%, p = 0.22, m = 12, n = 4). However, the HbT amplitude without astrocytic Ca^{2+} response was significantly lower than that with astrocytic Ca^{2+} response(0.42% ± 0.03% versus 1.15% ± 0.06%, first 3 versus last 3 stimulations, $p < 0.0001$, m = 12, n = 4) (Figure 4F), suggesting that astrocytes modulate the NVC response upon neuronal stimulation.

To attempt to sort out the responses of astrocyte soma from those of the processes, we measured the astrocytic Ca^{2+} increases to single stimulation after local cortical injection of carbenoxolone (Cbx) to inhibit gap junctions, which should influence astrocytic processes, and after cyclopiazonic acid (CPA) to deplete astrocyte intracellular Ca^{2+} stores, which would influence astrocytic somata (Kuga et al., 2011; Srinivasan et al., 2015). After Cbx, the response to single stimulation was almost completely abolished, from a baseline of 2.56% ± 0.05% to 0.075% ± 0.035% ($p < 0.0001$, m = 12, n = 3, Student's t test), whereas after CPA, the response was only partly reduced, to 1.28% ± 0.086% ($p < 0.001$, m = 12, n = 3,

Student's t test) (Figures 4K–4N). This is consistent with the interpretation that the transient Ca^{2+} evoked by single stimulation originated primarily from the fast astrocyte processes (Otsu et al., 2015). Although consistent with the notion that the astrocyte response to single stimulation is due to astrocyte processes, the Cbx application also affected neuronal responses (Figures 4G–4J), complicating the assumption that these agents are specific.

Overall, these results show that neuronal Ca^{2+} transients had a one-to-one association with the hemodynamic responses during continuous, low-frequency stimulation; astrocytic Ca^{2+} transients during single stimulation dissociated from the hemodynamic responses, their occurrences decreased following the first 3 stimulations in a trial, but when they occurred, they were associated with stronger hemodynamic responses; and the fast astrocytic Ca^{2+} activity appeared to be mediated by the processes of astrocytes and might be predominantly engaged at the onset of upcoming hemodynamic responses (e.g., the first 3 stimulations).

Neuronal Ca^{2+} Drives NVC under High-Frequency Stimulation, and Slow Astrocytic Ca^{2+} Is Associated with Vasoconstriction

Unlike previous studies that only observed strong high-frequency stimulation-evoked slow astrocytic Ca^{2+} elevations, our results showed that fast Ca^{2+} transients from synchronized astrocytic processes responded to the onset of single stimulations (as achieved at 0.3 Hz) but frequently disassociated from the ΔHbT responses after repeated stimulations (Figures 4B and 4C). We also showed that 5-Hz stimulations evoked both an early phase of fast transient-like Ca^{2+} and a later phase of slow cumulative astrocytic Ca^{2+} elevations (Figure 5G). The simultaneous assessment of the hemodynamic responses (e.g., ΔCBF, ΔHbT, and vessel diameter change [ΔD/D]) allowed us to assess the role of these astrocytic Ca^{2+} signals in NVC under fast stimulations.

A comparison of temporal profiles during high-frequency stimulation (5 Hz) showed that neuronal Ca^{2+} elevations correlated with the hemodynamic changes (e.g., ΔCBF, ΔHbT, and ΔD/D) despite delays in their onset (e.g., $\tau_{CBF} = 1.3 \pm 0.44$ s, $\tau_{HbT} = 3.24 \pm 0.53$ s, $\tau_{\Delta D/D} = 0.501 \pm 0.079$ s; n = 5 mice), all of which reached their peak and started to decrease near the end of the stimulation period (t = 10 s) (Figures 5H and 5J–M, blue bars). In contrast, the overall astrocytic Ca^{2+} elevations evoked by high-frequency stimulation were de-correlated from the hemodynamic changes during stimulation (Figures 5I–5M, pink bars). However, when the coexisting fast and slow astrocytic Ca^{2+} modes were considered, a detailed comparison revealed that the fast-process Ca^{2+} fluctuations lasting 3.48 ± 0.9 s (red arrow in Figure 5G and in the dashed blue box in Figure 5I) correlated with the rising phase of ΔCBF (red trace), which might suggest a role of astrocyte processes in facilitating onset of NVC during the early phase of high-frequency stimulation. On the other hand, the correlation between the hemodynamics and the neuronal versus the astrocytic Ca^{2+} accumulation (Figures 5H–5K) showed that the slow astrocytic Ca^{2+} elevation ($\tau_A = 5.74 \pm 0.43$ s) did not correlate with ΔCBF ($r = -0.049 \pm 0.23$, $p = 0.088$, m = 20, n = 5, Student's t test) or ΔHbT ($r = 0.015 \pm 0.08$, $p = 0.249$, m = 20, n = 5, Student's t test). In contrast, cumulative neuronal Ca^{2+} had a strong positive correlation with ΔCBF ($r = 0.77 \pm 0.13$, $p < 0.001$, m = 20, n = 5, Student's t test) and ΔHbT ($r = 0.34 \pm 0.38$, $p < 0.001$, m = 20, n = 5, Student's t test) (Figure 5M). Instead, the 3.48 ± 0.09 s-delayed astrocytic Ca^{2+} elevation, whose plateau

extended 20 s beyond the stimulation period, correlated with the vasoconstriction (ΔD/D, r = 0.66 ± 0.05, $p < 0.001$, m = 20, n = 6, Student's t test) that followed the peak of stimulation-induced vasodilation (4.78 ± 0.2 s latency) (Figure 5L). The correlation between neuronal Ca^{2+} elevation (Figure 5M) and ΔD/D was not significant ($r_N = 0.1 \pm 0.25$, $p = 0.548$, m = 20, n = 5, Student's t test).

These results suggest that, although neuronal populations are better correlated with NVC during high-frequency stimulation, the astrocytic transients (presumably processes) likely facilitate early vascular responses, and the large, slow cumulative astrocytic Ca^{2+} elevations (presumably from astrocytic somata) appear to mediate vasoconstriction upon termination of high-frequency stimulation, enabling recovery of NVC following high-frequency stimulation. The long tail of Ca^{2+} elevation extending beyond the stimulation train could result from the confounding effects of the relatively slow decay of GCaMP6f that would not allow for recovery during high-frequency stimulation and the averaging of Ca^{2+} dynamics over an extended response volume that may have different temporal characteristics.

To identify the origin of the bi-phasic astrocytic Ca^{2+} signal, we recorded the astrocytic Ca^{2+} increases to 5-Hz stimulations after local cortical injection of Cbx and CPA (Kuga et al., 2011; Srinivasan et al., 2015). Astrocytic slow cumulative Ca^{2+} elevation markedly decreased after CPA, from 4.7% ± 0.1% to 0.83% ±0.1% ($p < 0.0001$, m = 12, n = 3, two-tailed t test), whereas it did not change after Cbx (4.7% ± 0.1% to 4.5% ± 0.3%, $p = 0.67$, m = 12, n = 3, two-tailed t test) (Figure S5), which indicates that the soma drives cumulative Ca^{2+} during high-frequency stimulation. These results suggest that the slow accumulative Ca^{2+} phase likely originated primarily from the slow somatic signal of the astrocyte ensemble, as evidenced by its inhibition by CPA (Figure S5).

Resting State Neuronal, but Not Astrocytic, Ca^{2+} Slow Oscillations Correlated with Hemodynamic Slow Oscillations

Previous studies have found that the low-frequency oscillations (LFOs) used by resting fMRI to explore brain functional connectivity are most likely derived from neuronal activity (Du et al., 2014; Schölvinck et al., 2010). However, the interplay between neuronal and astrocytic activities giving rise to LFOs has not been studied. The resting LFOs of neuronal and of astrocytic Ca^{2+} signals and of the hemodynamic (e.g., HbT) fluctuations were measured (Figures 6A–6C) (the methods are described in Figure S6). The power spectra of resting LFOs in the synchronized neuronal or astrocytic Ca^{2+} signals were derived by Fourier transform, as shown in Figures 6D–6G (Du et al., 2014). Neuronal Ca^{2+}, HbT, and CBF all showed an LFO spectral peak within 0.03–0.08 Hz (cellular and metabolic band; black arrows in Figure 6), and CBF showed an additional peak (red arrow) around 0.1–0.12 Hz (vascular effect), as previously reported (Du et al., 2014). Astrocytic Ca^{2+} exhibited only narrow band responses that occasionally got above background noise but no prominent band of LFO between 0.03–0.08 Hz, as detected for neuronal and hemodynamic responses (Figure 6E).

The correlation between hemodynamic LFOs and neuronal (blue) versus astrocytic (purple) Ca^{2+} LFOs (Figure 6I) showed that neuronal Ca^{2+} LFO was correlated with ΔHbT LFO (r = 0.314 ± 0.051, $p = 0.016$, n = 6 mice), with a HbT time lag of 2.96 ± 0.32 s. There was no

significant correlation between astrocytic Ca^{2+} and HbT LFOs (r = 0.14 ± 0.04, p = 0.47, n = 6 mice). This result confirms that the cellular driver for resting LFOs (frequency f = 0.03–0.08 Hz) is the neurons and is consistent with prior studies that show correlations between low-frequency hemodynamic changes and low-frequency neuronal activities (Schölvinck et al., 2010; Shmuel and Leopold, 2008). We have now measured resting spontaneous astrocytic activity and shown that astrocytes do not contribute to resting LFOs.

All data described so far were acquired under normal physiological conditions. To test the effects of hypercapnia on the contribution of astrocytes to LFOs, inhaled CO_2 was increased, which dilated the cerebrovascular vessels. During hypercapnia, an LFO peak of astrocytic Ca^{2+} emerged within 0.03–0.08 Hz (Figure S6). This indicates that, although neuronal oscillatory activity correlated with hemodynamic LFOs, astrocytes might contribute to oscillatory signals when hemodynamics deviate from natural physiological states, such as is the case for vasodilation induced by hypercapnia, or, presumably, other disruptive physiological and/or pharmacological conditions. Other than the additional peak around 0.1–0.12 Hz (vascular effect), the hemodynamic fluctuations under hypercapnia remained largely unchanged; e.g., ΔHbT LFO from 17.3% ± 2.88% to 15.2% ± 0.49% (p = 0.135), ΔCBF LFO from 8.27% ± 1.73% to7.48% ± 4.23% (p = 0.711). These results suggest that, although astrocytes under physiological conditions do not contribute to resting hemodynamic LFOs, they might participate when hemodynamics are disrupted, which emphasizes the importance of controlling the physiological state of the animal when measuring astrocytic activities.

DISCUSSION

Here the roles of synchronized Ca^{2+} from neuron and astrocyte populations were measured using GCaMP6f and correlated with NVC. Key findings from these studies were as follows:

1. The use of an innovative multimodality imaging approach allowed us to record changes in synchronized Ca^{2+} signaling from neuronal and astrocytic ensembles and the concurrent hemodynamic changes at a higher temporal resolution (80-Hz sampling rate) and larger FOV (over 3 × $3mm^2$) than those of prior studies that used two-photon microscopy. The high sensitivity and fast frame rate enabled us to distinctly detect both astrocytic Ca^{2+} transients and slow accumulative responses. The data clearly show that, both in the resting state and during hind paw stimulation, NVC can occur without detectable astrocyte responses but that, when occurring, they affect the hemodynamic responses, suggesting that astrocyte responses are important for modulating NVC. When there was a fast transient astrocyte response (fast Ca^{2+} transient), NVC was stronger, and when strong stimulation triggered slow astrocyte responses (slow accumulative Ca^{2+}), there was vasoconstriction.

2. We characterized the neuronal and astrocytic Ca^{2+} transients using GCaMP6f, including latency, duration, and amplitude, and the frequency dependence of neuronal and astrocytic Ca^{2+} response that had not been previously reported. Importantly, detection of astrocytic Ca^{2+} transients in response to single sensory stimulation (e.g., 0.3 Hz) was possible because of the high sensitivity of MIP

combined with GCaMP6f. Although prior work reported rapid Ca^{2+} transients in astrocytes with a similar time course as neural Ca^{2+} signals, the data are confounded by the fact that they were acquired using bulk-loaded Ca^{2+} indicators, which are taken up by both neurons and astrocytes (Lind et al., 2013). In contrast, prior studies with two-photon microscopy (TPM) that used genetically encoded Ca^{2+} indicators were only able to detect responses triggered by fast stimulations; e.g., eight stimuli or more were needed to elicit robust responses (Haustein et al., 2014). More details regarding comparison with previous studies are provided in the Supplemental Experimental Procedures.

3. We characterized the relation between neuronal and astrocytic Ca^{2+} transients and the hemodynamic response (DHbT) to single sensory stimulation. The results show that the DHbT response is always associated with neuronal Ca^{2+} firing regardless of astrocytic Ca^{2+} activity. In addition, unlike previous studies (Schummers et al., 2008; Takano et al., 2006a), we documented that there was a relatively fast astrocytic Ca^{2+} response to single stimulation. A recent study combining fMRI and GCaMP6f recording of neurons and astrocytes reported that fast stimulation always elicited astrocytic activation that occurred in synchrony with BOLD responses (Wang et al., 2018). In our results, we also observed cumulative and extended astrocytic Ca^{2+} responses to all fast stimulations and uncovered an association with vasoconstriction after stimulation. As capillary responses are heterogeneous (some increase with vessel dilation and some may even decrease with vessel constriction) (Pan et al., 2014), flow measurements from a single capillary (e.g., with TPM) may also be subject to observation bias. In this respect, the ability to measure the changes in regional CBFv in response to stimulation-induced neuronal activation obviates this potential observation bias.

4. We found that, under high-frequency stimulation, astrocytic Ca^{2+} responses included an early-phase transient followed by a slow accumulation, which correlated with local microvascular constriction (i.e., possibly feedback to reset hemodynamics) after stimulation, and this was observed consistently for all high-frequency stimulation trains. We know of no other study demonstrating this temporal sequence in astrocytic Ca^{2+}, which transitions from low-amplitude fast spikes to cumulative high-amplitude Ca^{2+} responses with intermediate-frequency (5 Hz) and high-frequency stimulations.

5. Spontaneous LFOs using fMRI have been used to map brain functional connectivity based on the assumption that the hemodynamic (BOLD) LFOs represent the corresponding oscillatory fluctuations of intrinsic brain activity (White et al., 2009). Indeed, in a previous study, we showed that hemodynamic (e.g., HbR, the basis of BOLD) LFOs correlate with cellular (potentially including neuronal and astrocytic) Ca^{2+} LFOs (roughly 0.03–0.08 Hz) (Du et al., 2014). Later, Ma et al. (2016) used GCaMP6f to demonstrate that cellular LFO may be of neuronal origin, but the contribution of astrocytes to LFOs was not studied. Here, using high spatiotemporal resolution, simultaneous MIP images of hemodynamic and synchronized Ca^{2+} changes, we observed a frequency band at

~0.07 Hz in neuronal Ca^{2+} and HbT LFOs but not in astrocytic Ca^{2+}, indicating that the BOLD LFOs indeed reflect neuronal and not astrocytic activity. Interestingly, we also observed that a frequency band at ~0.07 Hz emerged in astrocytic Ca^{2+} LFOs under mild hypercapnia, suggesting a role for astrocytes in vasodilation. Altogether, our results, both at rest and during stimulation, expand our understanding of the role of astrocytes in NVC.

Synchronized Ca^{2+} Signaling from Neuronal versus Astrocytic Populations

Previous NVC research measuring Ca^{2+} changes has focused on single cells and single vessels using TPM imaging (Otsu et al., 2015; Schummers et al., 2008). These studies are critically important; however, large-scale cell ensembles may behave differently from any specific single cell and, thus, also need to be explored. This is especially true for understanding hemodynamic regulation where the vessel network is extensive. In several recent studies (Haustein et al., 2014; Paukert et al., 2014; Shigetomi et al., 2010, 2013; Srinivasan et al., 2015), genetically encoded Ca^{2+} indicators have shown great promise for studying astrocytic Ca^{2+} transients from subcellular regions, such as astrocytic processes, that were previously difficult to investigate (Srinivasan et al., 2015). In the current study, we used GCaMP6f to capture the fast transient Ca^{2+} responses of neurons and astrocytes (Chen et al., 2013). Using GCaMP6f injection, we uncovered different Ca^{2+} responses between neurons and astrocytes to sensory stimulation that were different over all frequencies used. The synchronized astrocytic Ca^{2+} responses were lower in amplitude than neuronal responses (1.74% ± 0.1% versus 6.40% ± 0.29%), had slower onsets (313 ± 65 ms versus 6.0 ± 2.7 ms), and were longer-lasting (993 ± 48 ms versus 537 ± 34 ms) and less synchronized (62.6% ± 9.1% broader than that of a single astrocyte versus similar neuronal Ca^{2+} transients for synchronized and single neurons). Most interestingly, the responses to single stimulation were very different. Although the neuronal population responded to virtually every stimulation under the conditions used (e.g., at 0.3 Hz), the astrocytes only responded 57.73% ± 8.2% of the time. The hemodynamic response, as measured by total hemoglobin, which represents blood volume, also responded to virtually every stimulation. This result clearly shows that NVC can occur without an astrocyte response. However, the amplitude of the hemodynamic response was larger when astrocytic Ca^{2+} increased, likely indicating that astrocytes play a modulatory role in NVC.

Because of sensitivity and resolution limitations of the MIP technique, we were unable to detect the response to individual neurons or astrocytes at subcellular resolutions and, instead, measured the synchronized responses of neuronal and astrocytic ensembles and the associated hemodynamic responses to single electrical stimulation. There are wider-field TPM techniques emerging that may allow both single-cell resolution and ensemble resolution; however, it is likely that, because of the nature of astrocyte gap junction coupling, it will be important to have information about the ensemble as well as about single cells. Indeed, there is a lot of literature documenting the advantages of detecting single neuronal activity as well as that of local field potential, which records ensemble activity. Generally, TPM has superb spatial resolution to image the dynamics of subcellular Ca^{2+} signaling, including that of astrocytic endfeet and the coupling effects of the neighboring individual blood vessels and nerves, but its FOV is very small. The MIP technique used in

this study offers great advantages for studying NVC over a larger FOV, with high sensitivity and high temporal resolution and allowing simultaneous recording of cellular and hemodynamic changes.

Prior *in vivo* studies using dye bulk loading of fluorescent indicators (Schummers et al., 2008) reported slow somatic Ca^{2+} elevations. However, recent studies have shown Ca^{2+} transients in astrocytic processes that are faster and more frequent and can occur independent of the astrocytic somatic signals (Srinivasan et al., 2015). The work presented here shows that the frequency of the stimulation also influences the type of astrocytic response elicited (fast versus slow and cumulative). Analyses of the association between the fast and slow astrocytic Ca^{2+} signals and the hemodynamic responses revealed that the fast astrocytic process signal tended to occur at the initiation of a new stimulation period, and when they occurred, the amplitude of the hemodynamic signal was larger than when they did not, suggesting a modulatory role in NVC. In contrast, the slow somatic Ca^{2+} signal was observed only for the higher-frequency stimulations (5–10 Hz) and was associated with a decrease in the hemodynamic response and correlated negatively with vessel diameter(i.e., vasoconstriction). This implicates a role of astrocytes in the resetting of vascular tone following vasodilation after high-frequency neuronal stimulations.

In our study, we also showed that GCaMP6f was expressed in pyramidal neurons (Figure S1), and, as reported by others, it was not expressed in interneurons (Wilson et al., 2017). A study by Lecrux et al. (2011) indicates that the vascular response is primarily driven by enhanced activity of output excitatory pyramidal neurons releasing glutamate and cyclooxygenase-2 (COX-2) products. Our findings are also consistent with pyramidal neurons being the neurogenic hubs of NVC in the somatosensory cortex. Previous studies have indicated that pyramidal neurons are neurogenic hubs and that interneurons are key intermediaries in NVC (Lecrux et al., 2011). Thus, new drugs and methods that block astrocyte gap junctions devoid of neuronal (pyramidal neurons and interneurons) or vascular effects need to be developed.

Studies have shown that astrocytes are functionally and structurally heterogeneous (Morel et al., 2017). The physiological diversity of astrocytes is apparent between different brain circuits and microcircuits, and individual astrocytes display diverse signaling in subcellular compartments (Bayraktar et al., 2014; Khakh and Sofroniew, 2015). We compared the astrocytic Ca^{2+} responses of several small ROIs with single (presumably fast subtype) and fast (presumably slow subtype) stimulations and showed that astrocytes within the same ROIs responded with Ca^{2+} transients to slow stimulations (0.3–1 Hz) and with slow Ca^{2+} accumulations to fast stimulations (5 Hz). Although unlikely because each ROI (e.g., ~ϕ50 mm) comprises few astrocytes, we cannot rule out the possibility that different subtypes might underlie the transient versus the accumulative Ca^{2+} responses. Future studies with subcellular imaging are needed to clarify whether Ca^{2+} transients to single stimulation occur in the same astrocytes that show accumulative responses with fast stimulation.

The following are limitations of our studies. Although we assign the synchronized astrocytic Ca^{2+} transient increases to processes and the slow large increase with high-frequency stimulation to somatic Ca^{2+} increases, our imaging approach lacked subcellular resolution to

reliably identify individual astrocyte processes and somatic signals. Instead, we provide evidence that the transient Ca^{2+} signals corresponded to astrocytic processes by their sensitivity to Cbx, whereas the demonstration that the slowcumulative Ca^{2+} fromsomata is supported by their sensitivity to CPA, as used previously (Srinivasan et al., 2015). Although Cbx is not ideal for studying the role of astrocytes in NVC because it also affects neuronal activities, which, in turn, would affect NVC (Selli et al., 2014), here we used it specifically to understand the fast astrocytic responses. Gap junction inhibitors that only affect astrocytes and not neurons are needed to affirmatively identify the roles of astrocytes in NVC. Improving the spatial resolution of our imaging setup with new capabilities (Boas and Dunn, 2010; Logothetis, 2008; White et al., 2009) is also needed to ultimately validate the kinetic differences of the responses to stimulations in subcellular astrocytic compartments. The slow off rate of GCaMP6f likely constrained the temporal resolution to distinguish very fast Ca^{2+} changes during fast (>1 Hz) stimulations (Chen et al., 2013). Another limitation was the use of anesthesia because anesthetics affect astrocytic Ca^{2+} signals (Takano et al., 2006a; Thrane et al., 2012). Details regarding the selection of anesthetics are addressed in Figure S7. Also, although inferring the lack of interaction between neuronal and astrocytic Ca^{2+} responses based on consistent neuronal responses to single stimulation and inconsistent ones in astrocytes, we were limited by the fact that we did not simultaneously record neuronal and astrocytic responses Ca^{2+} in the same animal.

Conclusions

The results show that a synchronized Ca^{2+} response can be detected from astrocytes in response to low-frequency sensory stimulation. At low frequencies, many stimulations did not evoke an astrocyte response, in contrast to the neuronal and hemodynamic responses. This indicates that the astrocyte response is not necessary to evoke a hemodynamic response even though the astrocyte response is fast enough. However, when astrocytes did respond, the hemodynamic response was larger, indicating a likely role in modulating the strength of NVC. At the higher frequencies, the slow and longer-lasting astrocytic Ca^{2+} accumulation (presumably of somatic origin), which was consistently elicited to fast stimulation, is likely to play a role in constricting dilated vessels following stimulation, mediating resetting of NVC. During resting conditions, there was very low power in slow astrocytic Ca^{2+} fluctuations, which did not correlate with the slow hemodynamic oscillations. This indicates that neuronal, but not astrocytic, fluctuations drive slow hemodynamic fluctuations in the resting state.

EXPERIMENTAL PROCEDURES

All experiments were carried out according to NIH guidelines and were approved by the Institutional Animal Care and Use Committee of Stony Brook University. The physiological conditions (electrocardiography [ECG], body temperature, respiration, partial pressure of carbon dioxide [pCO_2], partial pressure of oxygen [pO_2], and pH) were continuously monitored during the experiment to ensure a similar status for all mice (Figure S7; Table S1).

Transgenic Mice and GCaMP6f Expression in Neurons and Astrocytes

GFAP-Cre mice, obtained from Jackson Laboratory and maintained as a heterozygous line, were used for experiments when they reached an age between postnatal days 60–70 (P60–P70). All information regarding the generation and genotyping of this line is available at https://www.jax.org/strain/024098. To express GCaMP6f in astrocytes of the transgenic mouse brain, a virus, AAV5.CAG.Flex.GCaMP6f.WPRE.SV40 (AV-5-PV2816, Penn Vector Core), was injected into the hindpaw area of the sensorimotor cortex. To express GCaMP6f in neurons of the mouse brain, a virus, AAV5.Syn.GCaMP6f.WPRE.SV40 (AV-5-PV2822, Penn Vector Core), was injected into the same brain region of the wild-type (WT).

In Vivo Time-Lapse MIP Imaging

A custom MIP developed in our lab was used for simultaneous image acquisition of Ca^{2+} fluorescence, HbT, and CBFv in a time-sharing mode (Figure 1). For GCaMP6f-Ca^{2+} fluorescence imaging, a narrow-band blue light-emitting diode (LED) at 488 nm (Lumencor) was used for excitation, and a long-pass dichroic filter at 495 nm (Semrock, Rochester, NY) was used for fluorescence emission. The neuronal or astrocyte activity was quantified as ΔF/F after spectral absorption correction to minimize the confounding artifacts induced by the hemodynamic changes, such as in HbT, acquired at the isoseismic point of 568 nm. CBF was mapped by laser speckle contrast image (LSCI), which acquired photographic images illuminated by a laser diode at 830 nm through a bifurcated monomode fiber. The relative change of CBF (ΔCBF) was calculated from the speckle contrast coefficient, $K = \left\{\tau_c/T + \tau_c^2/2T^2[\exp(-2T/\tau_c) - 1]\right\}^{1/2}$, where σ is the local SD of the adjacent pixels' intensities from a sub-volume in the spatiotemporal domain, T is the camera exposure time, and $<I>$ denotes the mean value of the intensity from this sub-volume (Luo et al., 2008). CBF (relative flow rate) is inversely proportional to the decorrelation time τ_c. All channels of spectral illumination and image acquisition (time [T] = 10 ms exposure per channel) were controlled by a workstation via a high-speed digital time base using custom C++ software. The neuronal and astrocytic Ca^{2+} transients were imaged at 80 frames per second (fps), and the hemodynamic responses (e.g., HbT and CBF channels) were imaged at 12.5 fps. Paradigms for sensory stimulation and resting state oscillations are detailed in the Supplemental Experimental Procedures and Figure S6.

Statistics

All data are presented as means ± SEM. Comparison of two different groups (e.g., neurons and astrocytes) or two different time periods (pre- and post-stimulation) was analyzed using Student's t test when normality tests were passed; otherwise, a Mann-Whitney test was used as indicated. Comparisons made across multiple stimulation trials within a group (e.g., stimulation trial 1, 2,…, in neuron or astrocyte group) were analyzed using repeated measurement (RM) one-way ANOVA. If the p value is less than 0.001, then it is reported as $p < 0.001$; otherwise, precise p values are provided for each test. In all tests, $p < 0.05$ is considered statistically significant.

Supplementary Material

Refer to Web version on PubMed Central for supplementary material.

ACKNOWLEDGMENTS

We thank K. Park for assisting with animal handling and K. Clare and A. Chen for help with staining. This research was supported in part by NIH grants R01DA029718 and R21DA042597 (to Y.P. and C.D.), by Fundamental Research Funds for the Central Universities of China (to X.G.), and by NIH intramural programs (to N.D.V. and A.P.K.).

REFERENCES

Attwell D, and Laughlin SB (2001). An energy budget for signaling in the grey matter of the brain. J. Cereb. Blood Flow Metab 21, 1133–1145. [PubMed: 11598490]

Bayraktar OA, Fuentealba LC, Alvarez-Buylla A, and Rowitch DH (2014). Astrocyte development and heterogeneity. Cold Spring Harb. Perspect. Biol 7, a020362. [PubMed: 25414368]

Boas DA, and Dunn AK (2010). Laser speckle contrast imaging in biomedical optics. J. Biomed. Opt 15, 011109. [PubMed: 20210435]

Chen TW, Wardill TJ, Sun Y, Pulver SR, Renninger SL, Baohan A, Schreiter ER, Kerr RA, Orger MB, Jayaraman V, et al. (2013). Ultrasensitive fluorescent proteins for imaging neuronal activity. Nature 499, 295–300. [PubMed: 23868258]

Di Castro MA, Chuquet J, Liaudet N, Bhaukaurally K, Santello M, Bouvier D, Tiret P, and Volterra A (2011). Local Ca2+ detection and modulation of synaptic release by astrocytes. Nat. Neurosci 14, 1276–1284. [PubMed: 21909085]

Du C, Volkow ND, Koretsky AP, and Pan Y (2014). Low-frequency calcium oscillations accompany deoxyhemoglobin oscillations in rat somatosensory cortex. Proc. Natl. Acad. Sci. USA 111, E4677–E4686. [PubMed: 25313035]

Giaume C, Koulakoff A, Roux L, Holcman D, and Rouach N (2010). Astroglial networks: a step further in neuroglial and gliovascular interactions. Nat. Rev. Neurosci 11, 87–99. [PubMed: 20087359]

Girouard H, Bonev AD, Hannah RM, Meredith A, Aldrich RW, and Nelson MT (2010). Astrocytic endfoot Ca2+ and BK channels determine both arteriolar dilation and constriction. Proc. Natl. Acad. Sci. USA 107, 3811–3816. [PubMed: 20133576]

Gu X, Chen W, You J, Koretsky AP, Volkow ND, Pan Y, and Du C (2018). Long-term optical imaging of neurovascular coupling in mouse cortex using GCaMP6f and intrinsic hemodynamic signals. NeuroImage 165, 251–264. [PubMed: 28974452]

Haustein MD, Kracun S, Lu XH, Shih T, Jackson-Weaver O, Tong X, Xu J, Yang XW, O'Dell TJ, Marvin JS, et al. (2014). Conditions and constraints for astrocyte calcium signaling in the hippocampal mossy fiber pathway. Neuron 82, 413–429. [PubMed: 24742463]

Hirase H, Qian L, Barthó P, and Buzsáki G (2004). Calcium dynamics of cortical astrocytic networks in vivo. PLoS Biol. 2, E96. [PubMed: 15094801]

Khakh BS, and Sofroniew MV (2015). Diversity of astrocyte functions and phenotypes in neural circuits. Nat. Neurosci 18, 942–952. [PubMed: 26108722]

Kuga N, Sasaki T, Takahara Y, Matsuki N, and Ikegaya Y (2011). Large-scale calcium waves traveling through astrocytic networks in vivo. J. Neurosci 31, 2607–2614. [PubMed: 21325528]

Lecrux C, Toussay X, Kocharyan A, Fernandes P, Neupane S, Lévesque M, Plaisier F, Shmuel A, Cauli B, and Hamel E (2011). Pyramidal neurons are "neurogenic hubs" in the neurovascular coupling response to whisker stimulation. J. Neurosci 31, 9836–9847. [PubMed: 21734275]

Lind BL, Brazhe AR, Jessen SB, Tan FC, and Lauritzen MJ (2013). Rapid stimulus-evoked astrocyte Ca2+ elevations and hemodynamic responses in mouse somatosensory cortex in vivo. Proc. Natl. Acad. Sci. USA 110, E4678–E4687. [PubMed: 24218625]

Logothetis NK (2008). What we can do and what we cannot do with fMRI. Nature 453, 869–878. [PubMed: 18548064]

Luo Z, Wang Z, Yuan Z, Du C, and Pan Y (2008). Optical coherence Doppler tomography quantifies laser speckle contrast imaging for blood flow imaging in the rat cerebral cortex. Opt. Lett 33, 1156–1158. [PubMed: 18483544]

Ma Y, Shaik MA, Kozberg MG, Kim SH, Portes JP, Timerman D, and Hillman EM (2016). Resting-state hemodynamics are spatiotemporally coupled to synchronized and symmetric neural activity in excitatory neurons. Proc. Natl. Acad. Sci. USA 113, E8463–E8471. [PubMed: 27974609]

Metea MR, and Newman EA (2006). Glial cells dilate and constrict blood vessels: a mechanism of neurovascular coupling. J. Neurosci 26, 2862–2870. [PubMed: 16540563]

Mishra A, Reynolds JP, Chen Y, Gourine AV, Rusakov DA, and Attwell D (2016). Astrocytes mediate neurovascular signaling to capillary pericytes but not to arterioles. Nat. Neurosci 19, 1619–1627. [PubMed: 27775719]

Morel L, Chiang MSR, Higashimori H, Shoneye T, Iyer LK, Yelick J, Tai A, and Yang Y (2017). Molecular and Functional Properties of Regional Astrocytes in the Adult Brain. J. Neurosci 37, 8706–8717. [PubMed: 28821665]

Mulligan SJ, and MacVicar BA (2004). Calcium transients in astrocyte endfeet cause cerebrovascular constrictions. Nature 431, 195–199. [PubMed: 15356633]

Nimmerjahn A, and Bergles DE (2015). Large-scale recording of astrocyte activity. Curr. Opin. Neurobiol 32, 95–106. [PubMed: 25665733]

Nimmerjahn A, Mukamel EA, and Schnitzer MJ (2009). Motor behavior activates Bergmann glial networks. Neuron 62, 400–412. [PubMed: 19447095]

Nizar K, Uhlirova H, Tian P, Saisan PA, Cheng Q, Reznichenko L, Weldy KL, Steed TC, Sridhar VB, MacDonald CL, et al. (2013). In vivo stimulus-induced vasodilation occurs without IP3 receptor activation and may precede astrocytic calcium increase. J. Neurosci 33, 8411–8422. [PubMed: 23658179]

Nuriya M, and Hirase H (2016). Involvement of astrocytes in neurovascular communication. Prog. Brain Res 225, 41–62. [PubMed: 27130410]

O'Herron P, Chhatbar PY, Levy M, Shen Z, Schramm AE, Lu Z, and Kara P (2016). Neural correlates of single-vessel haemodynamic responses in vivo. Nature 534, 378–382. [PubMed: 27281215]

Otsu Y, Couchman K, Lyons DG, Collot M, Agarwal A, Mallet JM, Pfrieger FW, Bergles DE, and Charpak S (2015). Calcium dynamics in astrocyte processes during neurovascular coupling. Nat. Neurosci 18, 210–218. [PubMed: 25531572]

Pan Y, You J, Volkow ND, Park K, and Du C (2014). Ultrasensitive detection of 3D cerebral microvascular network dynamics in vivo. Neuroimage 103, 492–501. [PubMed: 25192654]

Panatier A, Vallée J, Haber M, Murai KK, Lacaille JC, and Robitaille R (2011). Astrocytes are endogenous regulators of basal transmission at central synapses. Cell 146, 785–798. [PubMed: 21855979]

Paukert M, Agarwal A, Cha J, Doze VA, Kang JU, and Bergles DE (2014). Norepinephrine controls astroglial responsiveness to local circuit activity. Neuron 82, 1263–1270. [PubMed: 24945771]

Rosenegger DG, and Gordon GR (2015). A slow or modulatory role of astrocytes in neurovascular coupling. Microcirculation 22, 197–203. [PubMed: 25556627]

Schölvinck ML, Maier A, Ye FQ, Duyn JH, and Leopold DA (2010). Neural basis of global resting-state fMRI activity. Proc. Natl. Acad. Sci. USA 107, 10238–10243. [PubMed: 20439733]

Schulz K, Sydekum E, Krueppel R, Engelbrecht CJ, Schlegel F, Schröter A, Rudin M, and Helmchen F (2012). Simultaneous BOLD fMRI and fiber-optic calcium recording in rat neocortex. Nat. Methods 9, 597–602. [PubMed: 22561989]

Schummers J, Yu H, and Sur M (2008). Tuned responses of astrocytes and their influence on hemodynamic signals in the visual cortex. Science 320, 1638–1643. [PubMed: 18566287]

Selli C, Erac Y, and Tosun M (2014). Cyclopiazonic acid alters serotonin-induced responses in rat thoracic aorta. Vascul. Pharmacol 61, 43–48. [PubMed: 24704610]

Shigetomi E, Kracun S, Sofroniew MV, and Khakh BS (2010). A genetically targeted optical sensor to monitor calcium signals in astrocyte processes. Nat. Neurosci 13, 759–766. [PubMed: 20495558]

Shigetomi E, Bushong EA, Haustein MD, Tong X, Jackson-Weaver O, Kracun S, Xu J, Sofroniew MV, Ellisman MH, and Khakh BS (2013). Imaging calcium microdomains within entire astrocyte

territories and endfeet with GCaMPs expressed using adeno-associated viruses. J. Gen. Physiol 141, 633–647. [PubMed: 23589582]

Shigetomi E, Patel S, and Khakh BS (2016). Probing the Complexities of Astrocyte Calcium Signaling. Trends Cell Biol. 26, 300–312. [PubMed: 26896246]

Shmuel A, and Leopold DA (2008). Neuronal correlates of spontaneous fluctuations in fMRI signals in monkey visual cortex: Implications for functional connectivity at rest. Hum. Brain Mapp 29, 751–761. [PubMed: 18465799]

Srinivasan R, Huang BS, Venugopal S, Johnston AD, Chai H, Zeng H, Golshani P, and Khakh BS (2015). Ca(2+) signaling in astrocytes from Ip3r2(−/−) mice in brain slices and during startle responses in vivo. Nat. Neurosci 18, 708–717. [PubMed: 25894291]

Takano T, Tian GF, Peng W, Lou N, Libionka W, Han X, and Nedergaard M (2006a). Astrocyte-mediated control of cerebral blood flow. Nat. Neurosci 9, 260–267. [PubMed: 16388306]

Takata N, and Hirase H (2008). Cortical layer 1 and layer 2/3 astrocytes exhibit distinct calcium dynamics in vivo. PLoS ONE 3, e2525. [PubMed: 18575586]

Thrane AS, Rangroo Thrane V, Zeppenfeld D, Lou N, Xu Q, Nagelhus EA, and Nedergaard M (2012). General anesthesia selectively disrupts astrocyte calcium signaling in the awake mouse cortex. Proc. Natl. Acad. Sci. USA 109, 18974–18979. [PubMed: 23112168]

Wang X, Lou N, Xu Q, Tian GF, Peng WG, Han X, Kang J, Takano T, and Nedergaard M (2006). Astrocytic Ca2+ signaling evoked by sensory stimulation in vivo. Nat. Neurosci 9, 816–823. [PubMed: 16699507]

Wang M, He Y, Sejnowski TJ, and Yu X (2018). Brain-state dependent astrocytic Ca^{2+} signals are coupled to both positive and negative BOLD-fMRI signals. Proc. Natl. Acad. Sci. USA 115, E1647–E1656. [PubMed: 29382752]

White BR, Snyder AZ, Cohen AL, Petersen SE, Raichle ME, Schlaggar BL, and Culver JP (2009). Resting-state functional connectivity in the human brain revealed with diffuse optical tomography. Neuroimage 47, 148–156. [PubMed: 19344773]

Wilson DE, Smith GB, Jacob AL, Walker T, Dimidschstein J, Fishell G, and Fitzpatrick D (2017). GABAergic Neurons in Ferret Visual Cortex Participate in Functionally Specific Networks. Neuron 93, 1058–1065.e4. [PubMed: 28279352]

Highlights

- Neurovascular coupling without astrocytic Ca^{2+} during slow somatosensory stimulation
- Neurovascular response is larger when astrocytic Ca^{2+} responds with slow stimulation
- Large increases in astrocytic Ca^{2+} occur with vasoconstriction with fast stimulation
- Low-frequency vascular fluctuations correlate with neuronal but not astrocytic Ca^{2+}

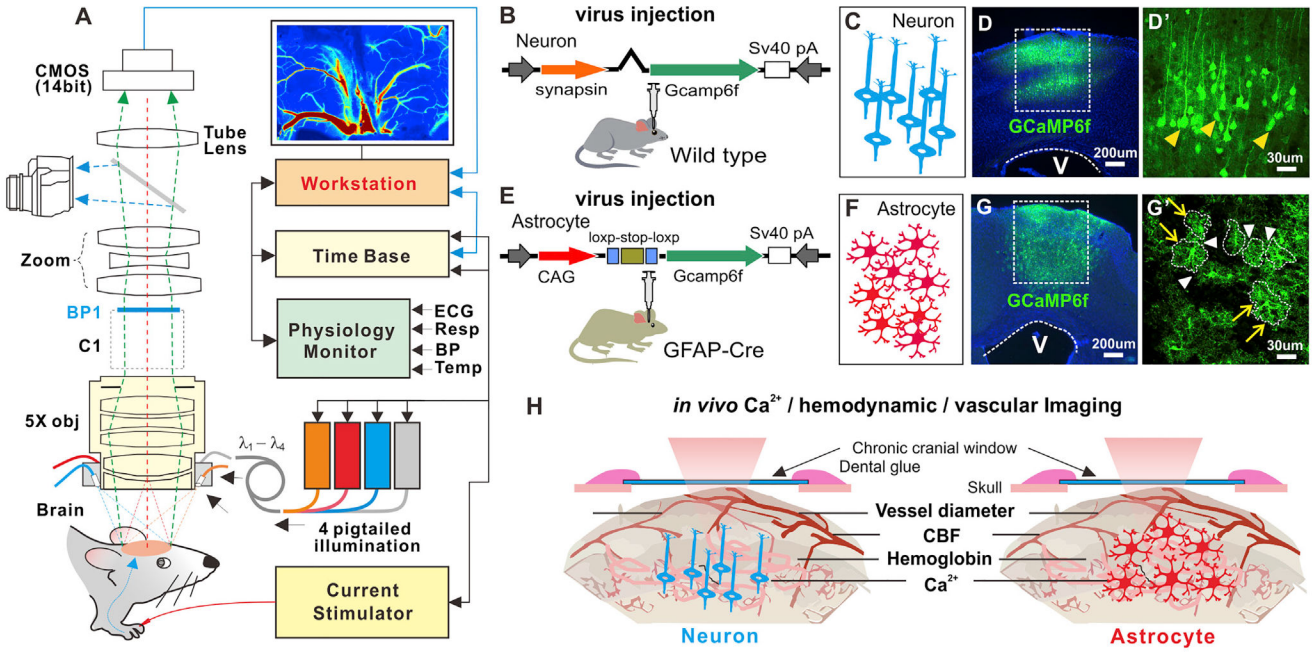

Figure 1. A Schematic Illustrating the Experimental Approach

(A) Multimodality imaging platform (MIP) that combines fluorescence, spectroscopic, and laser speckle contrast images for simultaneous cellular Ca^{2+} and hemodynamic recordings.

(B and E) Viral injection to express GCaMP6f in neurons and astrocytes, respectively.

(C and F) Cartoons representing neurons and astrocytes.

(D, D', G, and G') *Ex vivo* confocal fluorescence images showing the GCaMP6f distributions in cortical neurons and astrocytes (yellow arrows), where the dashed lines in (G) show the territories of astrocytes, with white arrows pointing to the connectivity between astrocytes.

(H) A sketch illustrating simultaneous MIP imaging of the synchronized Ca^{2+} from the neuronal or astrocytic network, CBF, HbT, and vessel dilation.

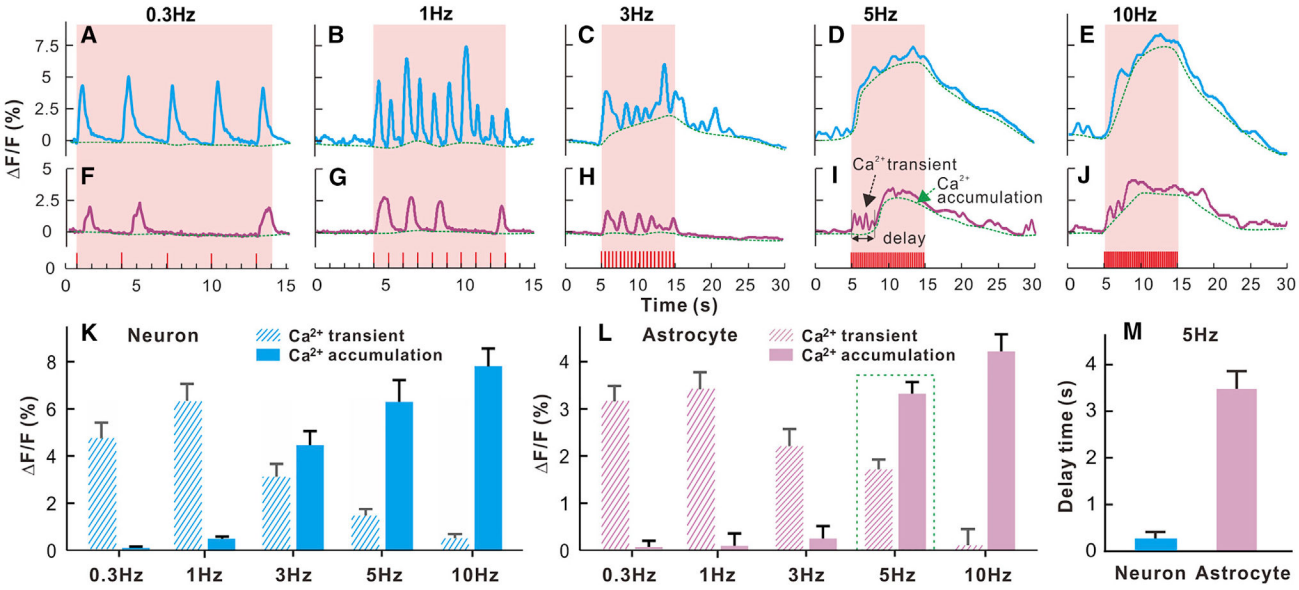

Figure 2. Frequency Dependence of Neuronal and Astrocytic Ca^{2+} Dynamics to Sensory Stimulations (3 mA and 0.3 ms)

(A–E) Synchronized neuronal Ca^{2+} responses to 0.3-, 1-, 3-, 5-, and 10-Hz stimulations.

(F–J) The corresponding astrocytic Ca^{2+} responses, showing predominance of fast transient Ca^{2+} at low frequency (single stimulation; e.g., 0.3 Hz) and slow cumulative Ca^{2+} at high frequency (fast stimulation; e.g., R5 Hz).

(K–M) Neuronal (transient and cumulative) Ca^{2+} (K) and astrocytic (transient and cumulative) (L) Ca^{2+} fluorescence amplitudes versus stimulation frequency and latencies to the onset of neuronal versus astrocytic Ca^{2+} cumulation evoked by 5Hz fast stimulation (M). The data are shown as mean ± SEM.

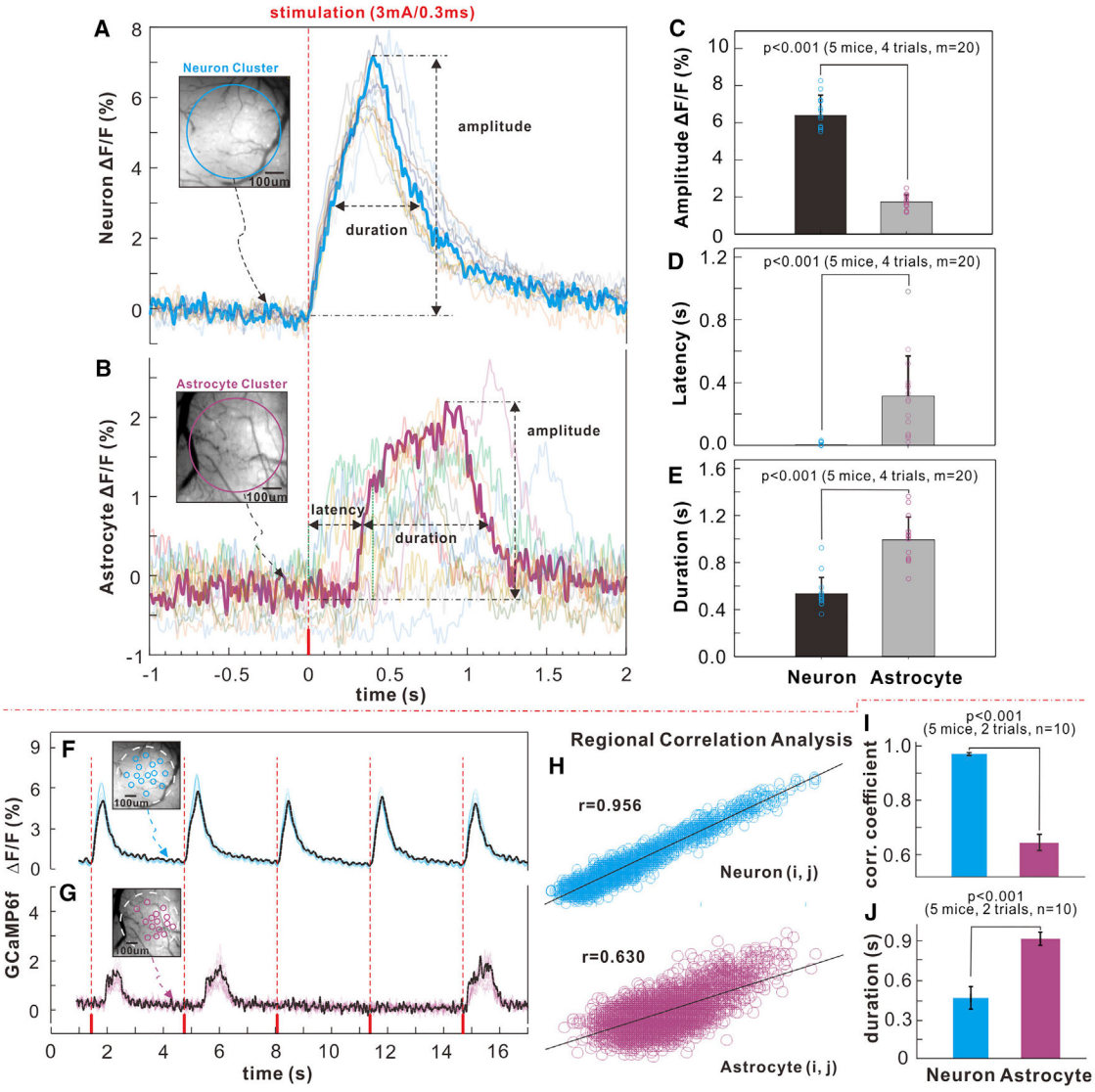

Figure 3. Synchronized Ca^{2+} Transients from Neuron and Astrocyte Populations Elicited by Single Sensory Stimulation (Hind Paw, 3 mA and 0.3 ms)

(A and B) Recorded neuronal and astrocytic Ca^{2+} traces of individual stimulations (m = 20) and their averaged traces (bold curves); the insets show the neuronal and astrocytic GCaMP6f fluorescence images.

(C–E) Statistical comparisons of amplitude, latency, and duration between neuronal and astrocytic GCaMP6f Ca^{2+} fluorescence transients.

(F and G) Traces of Ca^{2+} transients in single-cell ROIs (m = 15) elicited by a sensory stimulation for neuronal and astrocyte populations; small circles (~ϕ30 mm each, m = 15) represent the ROIs (blue for neurons, red for astrocytes) selected for cross-correlation analysis.

(H and I) Cross-correlation charts (i, j = 1,…,m) for neuronal and astrocyte populations and spatiotemporal correlations of neuronal and astrocytic Ca^{2+} transients.

(J) Durations of neuronal and astrocytic Ca^{2+} responses of single cells within the ROIs. The data are shown as mean ± SEM.

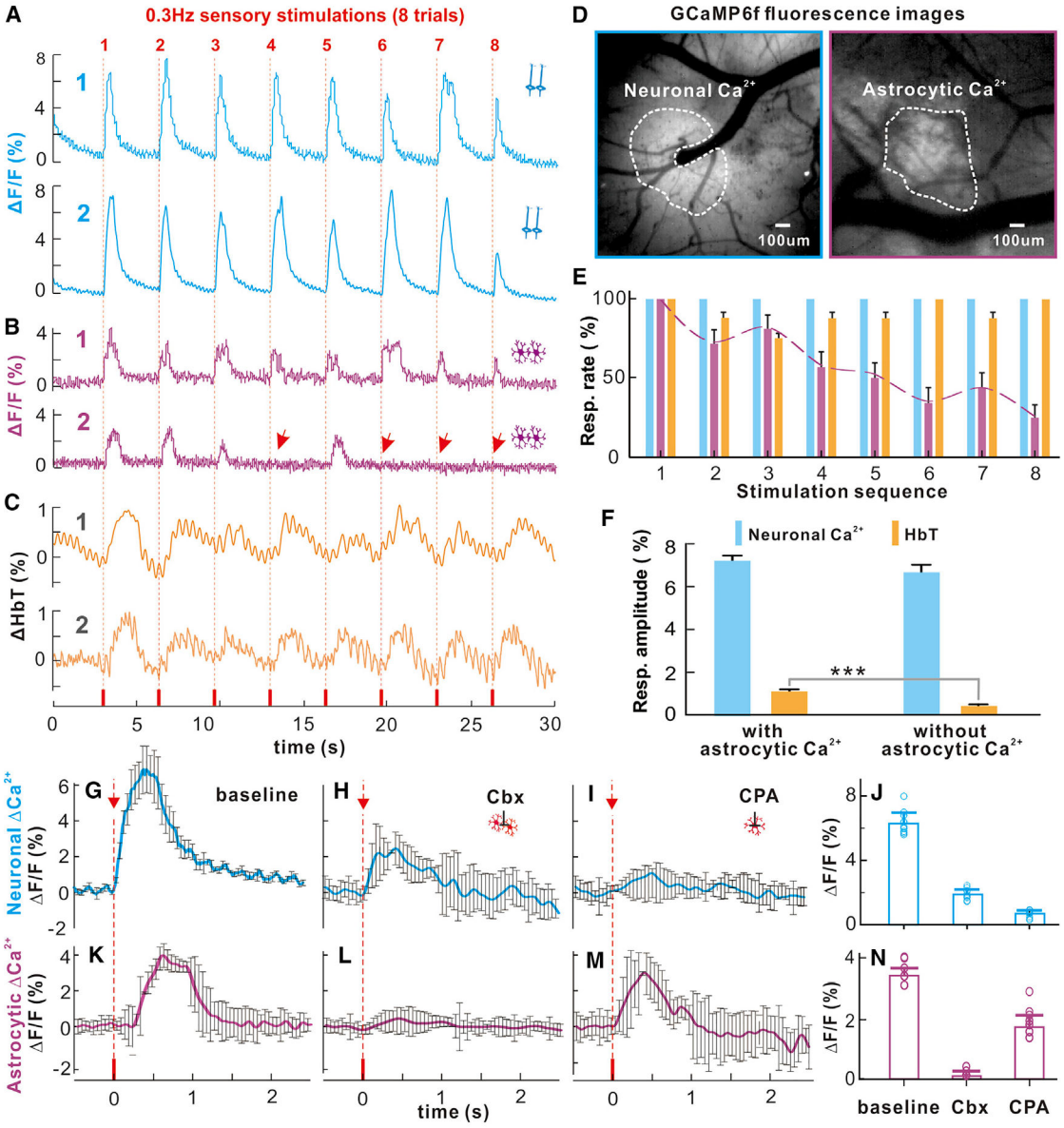

Figure 4. Traces of Synchronized Neuronal and Astrocytic Ca^{2+} and HbT Responses to a 0.3-Hz Sensory Stimulation Train (0.3 ms and 3 mA, 8 Trials)

(A) Synchronized neuronal Ca^{2+} (n = 2).

(B) Synchronized astrocytic Ca^{2+} (n = 2); arrows show missing responses.

(C) Hemodynamic responses (n = 2).

(D) ROIs.

(E) Mean response rates with stimulation trials, among which astrocytic Ca^{2+} response rates decreased with the stimulations.

(F) Neuronal Ca^{2+} and HbT amplitudes in response to stimulations with versus without astrocytic Ca^{2+} response (m = 4).

(G–I) Neuronal response to single stimulation at baseline and after topical cortical injection of Cbx and CPA applications.

(J) Histograms showing peak responses of neuronal Ca^{2+} (ΔF/F) under single stimulation, revealing significant differences from baseline to Cbx (i.e., 6.29% ± 0.2% versus 1.8% ± 0.08%, $p < 0.0001$, m = 12, n = 3, two-tailed t test) and from baseline to CPA (i.e., 6.29% ± 0.2% versus 0.64% ± 0.05%, $p < 0.0001$, m = 12, n = 3, two-tailed t test).
(K–M) Astrocytic Ca^{2+} transients to single sensory stimulation at baseline, after Cbx (i.e., 2.56% ± 0.05% versus 0.075% ± 0.035%, $p < 0.0001$, m = 12, n = 3, Student's t test) to inhibit gap junctions and of CPA (i.e., 2.56% ± 0.05% versus 1.28% ± 0.086%, $p < 0.0001$, m = 12, n = 3, Student's t test) to partially delete intracellular calcium (Ca^{2+}_i) stores and their statistics.
(N) Overall, Cbx abolished astrocytic Ca^{2+} transients, potentially suggesting that the fast astrocytic Ca^{2+} signaling might be from astrocyte processes (or endfeet). However, the assessment of the consequences of Ca^{2+} transient inhibition on NVC is confounded by the fact that Cbx also affected neuronal responses.

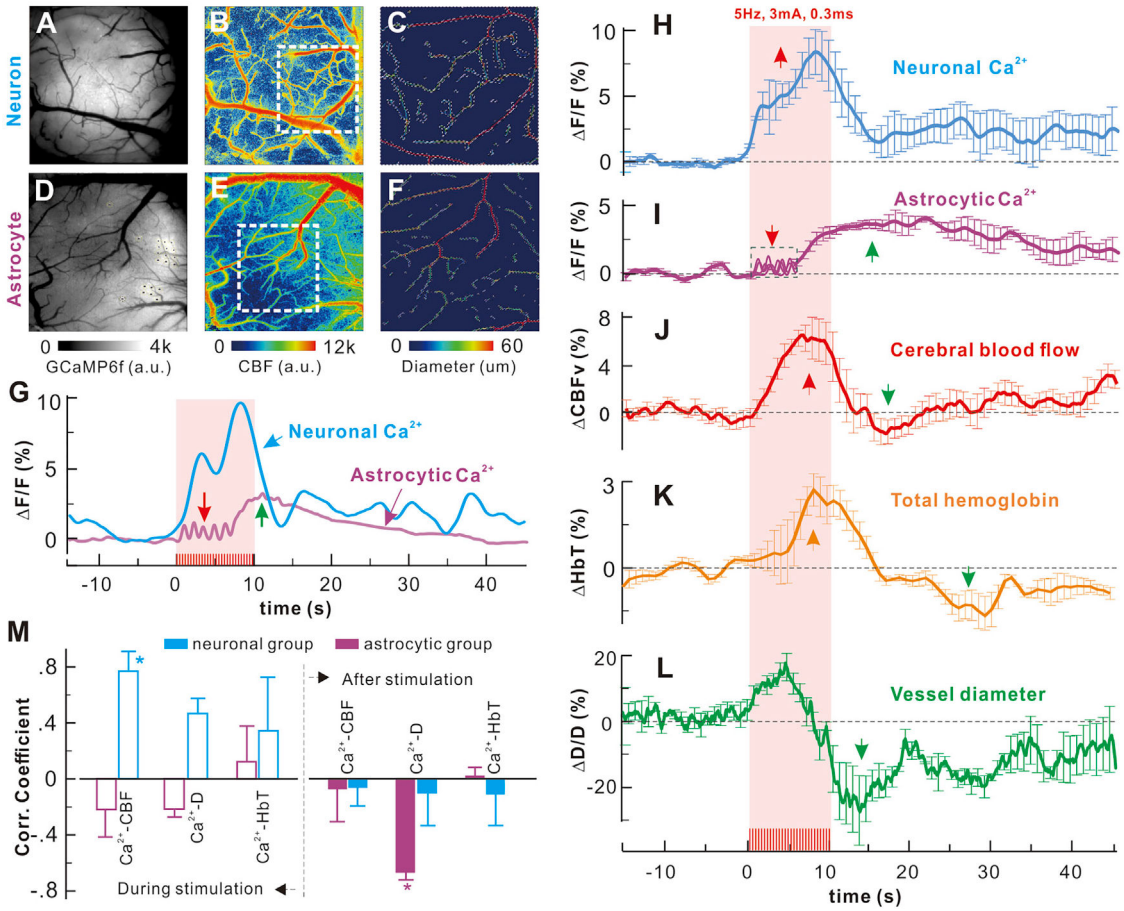

Figure 5. Synchronized Neuronal/Astrocytic Ca^{2+} and HbT Responses to 5-Hz Fast Sensory Stimulation (0.3 ms and 3 mA and 10 s)

(A–C) Neuronal Ca^{2+}, CBF, and angiographic images.

(D–F) Astrocytic Ca^{2+}, CBF, and angiographic images.

(G) Time-lapse neuronal or astrocyte Ca^{2+} elevations; the red and purple arrows point to the early phase of the fast process and later phase of slow cumulative somatic responses.

(H–L) Simultaneous acquisition of averaged time-lapse neuronal or astrocytic Ca^{2+} and hemodynamic (ΔCBF, ΔHbT, and ΔD/D) responses to fast stimulation (6 unaveraged traces in the dashed box in I), showing fast processes Ca^{2+}).

(M) Correlations of neuronal or astrocytic Ca^{2+} with ΔCBF, ΔHbT, ΔD/D during and after stimulation. The findings for the astrocytic Ca^{2+} elevations to 5-Hz stimulation at baseline and after topical cortical injection of Cbx and CPA, along with the corresponding neuronal Ca^{2+} changes, are shown in Figure S5.

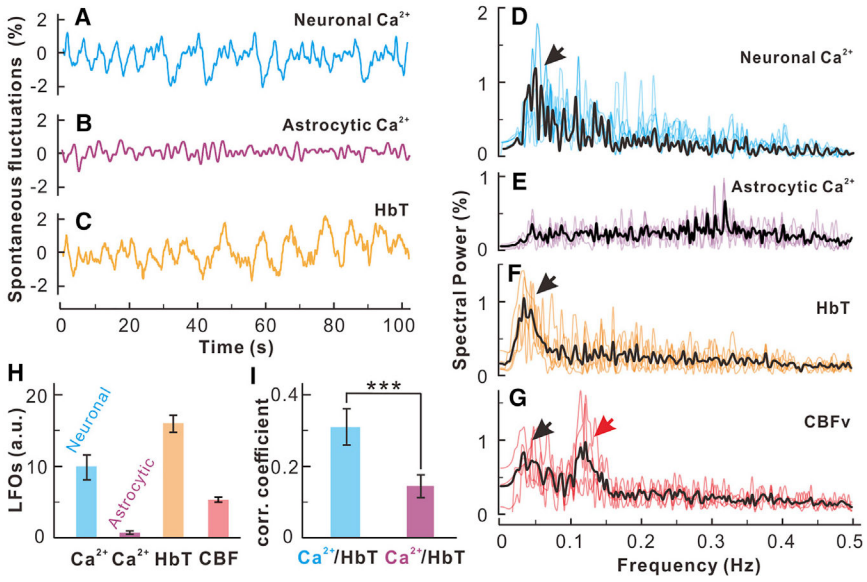

Figure 6. Resting State Neuronal but Not Astrocytic Ca^{2+} Slow Oscillations Correlated with Hemodynamic Slow Oscillations

(A–C) Time traces of resting state low-frequency oscillations in synchronized neuronal Ca^{2+} (blue), astrocytic Ca^{2+} (pink), and HbT (red) acquired from the sensorimotor cortex.

(D–G) Power spectra of LFOs of synchronized neuronal Ca^{2+}, synchronized astrocytic Ca^{2+}, HbT, and CBFv of the surrounding cortical parenchymal tissue.

(H) Statistical comparisons of LFO amplitudes within its oscillation band (0.03–0.08 Hz) under normocapnia averaged across animals (n = 6 mice).

(I) Correlation of neuronal Ca^{2+} and HbT (blue bar) versus astrocytic Ca^{2+} and HbT (purple bar) ($p = 0.014$, n = 6 mice).

The data are shown as mean ± SEM. Black/red arrows, lower band (0.04–0.08 Hz) and higher-band (~0.12 Hz) slow oscillations. The results for the resting-state LFOs under hypercapnia, performed to assess the response of astrocytic LFOs during vasodilation, are shown in Figure S6.